Exploring the power-limit of multi-modes multi-electrodes vibration energy harvesters

Adrien Morel, David Gibus, Adrien Badel

Exploring the power-limit of multi-modes multi-electrodes vibration energy harvesters

Adrien Morel
SYMME
Univ. Savoie Mont Blanc
Annecy, France
adrien.morel@univ-smb.fr

David Gibus
SYMME
Univ. Savoie Mont Blanc
Annecy, France
david.gibus@univ-smb.fr

Adrien Badel
SYMME
Univ. Savoie Mont Blanc
Annecy, France
adrien.badel@univ-smb.fr

***Abstract*— In this article, we propose a model for multi-modes multi-electrodes piezoelectric energy harvester, and study its dynamics when associated with an electrical interface. We show that a multi-modes harvester allows to overcome the traditional power limit defined for single-mode harvesters, thanks to the effect of the second mode on the first one. We investigate this phenomenon with a resistive load, both theoretically and experimentally, for a piezoelectric energy harvester made with an inverted mass and four pairs of piezoelectric electrodes. Multi-modes resonances allow to fully exploit the potential of multi-modes energy harvesters, and open ways to design large bandwidth large power density energy harvesters.**

Keywords*— *Vibrations, Energy harvesting, Piezoelectricity, Coupled dynamics, Multi-modes, Wideband, Resonance.

I. Introduction

Piezoelectric energy harvesters (PEH) have been widely used in order to harness energy from ambient vibrations and supply low-power electronic systems. PEH are usually made of a mechanical resonator that efficiently converts the ambient vibration in a strain applied on piezoelectric electrode(s), as long as the vibration frequency remains relatively close to the resonance frequency of the first mode [1]. The mechanical [2] and electrical [3, 4] optimization of the harvested power with such PEH has been widely investigated in the literature. An expression of the power limit that can be scavenged with such PEH has been derived, and illustrates that the maximum power that can be harvested with a PEH is proportional to its quality factor, to its effective mass, and to the squared vibration amplitude [5, 6, 7]. In this paper, we prove both theoretically and experimentally that the traditional power limit can be overcome, thanks to multi-modes multi-electrodes PEH.

Multi-modes PEH have been investigated in the last decades to obtain relatively large power bandwidth PEH and to harvest energy from broadband vibrations [8, 9, 10]. For instance, [8] proposed an L-shaped energy harvester whose second natural frequency is relatively close to the first one ($f_2/f_1 \approx 2$). [9] designed a PEH made of an array of cantilevers with different frequency responses that are all fixed on the same rigid base. Such approach allows to easily bring closer the modes frequencies and to widen the harvesting bandwidth at the cost of a larger size and lower power density. [10] proposed the analysis of a N degree-of-freedom (DOF) PEH made with multiple small masses fixed on a single large mass. It is notably shown that it is possible to dimension such structure in order to obtain multiple close peaks in the power response. To date, however, most multi-modes PEH analysis in the literature do not take into account the influence of the electrical interface on the PEH dynamics, and the coupling between the resonance modes that might appear due to this electrical interface.

In this paper, we propose to analyze multi-modes multi-ports PEH with coupled electrical interfaces. We first show that the traditional power limit, defined for single-mode single-port PEH, can be overcome thanks to multi-modes resonances. Thereafter, we prove, both theoretically then experimentally, that the effect of closer modes on single-mode resonance can appear with a well-chosen resistive interface. This proves that multi-modes PEH can be used not only to widen the harvesting bandwidth, but also to increase the power density of PEH.

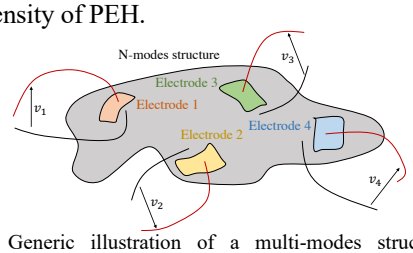

Figure 1: Generic illustration of a multi-modes structure with four piezoelectric electrodes.

II. Dynamics of Multi-modes Multi-electrodes PEH

A. Electromechanical model

In this paper, we consider a resonant structure with N resonance modes and covered by M piezoelectric electrodes driven by ambient acceleration (Fig.1). Assuming that the structure behaves linearly, the n^{th} mode of the structure ($\forall n \in [1, N]$)can be associated with an equivalent stiffness K_n, an equivalent linear damper D_n, an equivalent mass M_n, and an equivalent force factor B_{f_n}. The m^{th} piezoelectric electrode ($\forall m \in [1, M]$) impacts the n^{th} mode dynamics with an electrically-induced force $F_{nm} = \alpha_{nm} v_m$, with v_m being the voltage across the m^{th} piezoelectric electrode and α_{nm} the piezoelectric coefficient (force factor) between the m^{th} piezoelectric electrode and the n^{th} resonance mode. Note that $B_{f_n} \neq M_n$ as detailed in [11]. Thus, the dynamics of the n^{th} mode is governed by (1),

$$M_n \ddot{x}_n + D_n \dot{x}_n + K_n x_n + \sum_{m=1}^{M} \alpha_{nm} v_m = -B_{f_n} \gamma \qquad (1)$$

with x_n the displacement of the inertial mass of the resonator due to the n^{th} mode, and γ the base acceleration of the structure. The m^{th} piezoelectric electrode is under strain, which generates electrical charges and contributes to the evolution of the m^{th} voltage, v_m. Since all modes contribute to the strain of the m^{th} piezoelectric electrode, the equation governing the evolution of the voltage is given by (2),

$$i_m = C_{p_m} \dot{v}_m - \sum_{n=1}^{N} \alpha_{nm} \dot{x}_n \qquad (2)$$

with C_{p_m} and i_m the capacitance and the electrical current flowing out from the m^{th} piezoelectric electrode, respectively. The dynamics of a N -modes M -electrodes

This project has received funding from the European Union's Horizon 2020 research and innovation programme under grant agreement No 862289.

structures can be expressed thanks to N mechanical equations (1) and M electrical equations (2), and the equivalent circuit model of such harvester is shown in Fig.2.

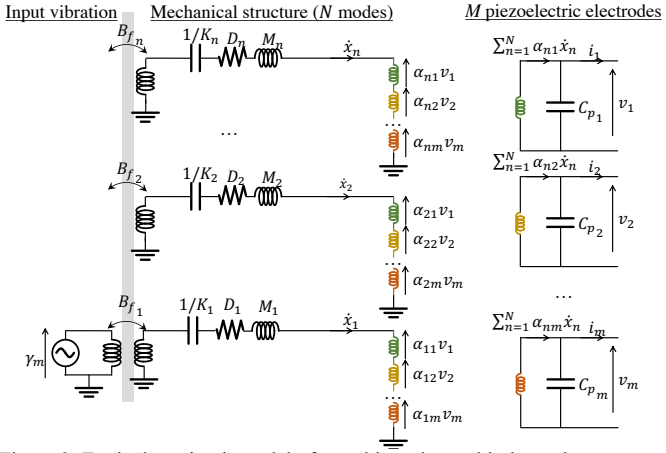

Figure 2: Equivalent circuit model of a multi-modes multi-electrodes energy harvester

B. Boundaries of the harvested power

The extracted power from the harvester P_{ext} can be calculated from the total power extracted from the M electrodes (3).

$$P_{ext} = \sum_{m=1}^{M} P_{ext,m} = \sum_{m=1}^{M} \frac{1}{T}\int_0^T i_m v_m \, dt \tag{3}$$

T being the period of the periodic excitation. Replacing i_m by its expression (2) yields (4).

$$P_{ext} = \frac{1}{T}\sum_{m=1}^{M}\int_0^T \left[C_{p_m}\dot{v}_m - \sum_{n=1}^{N}\alpha_{nm}\,\dot{x}_n\right] v_m \, dt \tag{4}$$

Since v_m is a T-periodic function, $\int_0^T \dot{v}_m v_m \, dt = 0$. Thus, the expression of the harvested power becomes (5).

$$P_{ext} = -\frac{1}{T}\sum_{n=1}^{N}\sum_{m=1}^{M}\int_0^T \alpha_{nm} v_m \, \dot{x}_n dt \tag{5}$$

Combining (1) with (5) and considering that x_n is a T-periodic function ($\int_0^T \dot{x}_n x_n \, dt = \int_0^T \ddot{x}_n \dot{x}_n \, dt = 0$) yields (6).

$$P_{ext} = \frac{1}{T}\sum_{n=1}^{N}\int_0^T \dot{x}_n \left[B_{f_n}\gamma + D_n \, \dot{x}_n\right] dt \tag{6}$$

In the case of a harmonic excitation, $\gamma(t) = \gamma_m \cos(\omega t)$. Since x_n is a T-periodic function $x_n = \sum_{k=1}^{+\infty}[a_k^n \cos(k\omega t) + b_k^n \sin(k\omega t)]$, with a_k^n and b_k^n the coefficients giving the in-phase and out-of-phase components of the k^{th} harmonic of x_n, respectively. The derivative of x_n, $\dot{x}_n$, can be expressed by $\dot{x}_n = \omega k \sum_{k=1}^{+\infty}[-a_k^n \sin(k\omega t) + b_k^n \cos(k\omega t)]$. Combining these expressions with (6) and using Parseval equality lead to the power expression (7).

$$P_{ext} = \frac{\omega}{2}\sum_{n=1}^{N}\left[\gamma_m a_1^n B_{f_n} - \omega D_n \sum_{k=1}^{+\infty} k^2\left[a_k^{n2} + b_k^{n2}\right]\right] \tag{7}$$

P_{ext} is maximized if the optimality conditions given by (8) are respected,

$$\begin{cases} \forall n, \quad a_1^n = \dfrac{\gamma_m B_{f_n}}{2\omega D_n} = \dfrac{\gamma_m B_{f_n} Q_n}{2\Omega_n M_n \omega_n^2} \\ \forall k > 1, \forall n, \quad a_k^n = 0 \\ \forall k > 0, \forall n, \quad b_k^n = 0 \end{cases} \tag{8}$$

with $Q_n = D_n^{-1}\sqrt{M_n K_n}$ the quality factor of the n^{th} mode, $\omega_n = \sqrt{K_n/M_n}$ the resonance pulsation of the n^{th} mode, and $\Omega_n = \omega/\omega_n$ the normalized vibration frequency. If the conditions given by (8) are respected, the harvested power is equal to the power limit of the harvester P_{lim}, whose expression is given by (9),

$$P_{lim} = \frac{\gamma_m^2}{4}\sum_{n=1}^{N}\frac{B_{f_n}^2 Q_n}{M_n \omega_n} = \sum_{n=1}^{N} P_{lim}^n \tag{9}$$

with P_{lim}^n the single-mode traditional power limit valid for the n^{th} resonance mode [5]. Some conclusions can be drawn from (7), (8) and (9):

- The optimal displacement waveform is a sine wave (in the case of harmonic excitation) whose phase-shift with the excitation is equal to 90°, and whose amplitude depends on the considered mode and on the excitation of amplitude.
- The higher harmonics of the mechanical displacement always decrease the harvested power. This means that electrical non-linearities (with circuits such as SECE and SSHI [5]) or mechanical non-linearities (with multi-stable harvesters, or stiffening/hardening behaviors [12]) might reduce the harvested power and unable to reach the power limit. However, in most case, the impact of the higher harmonics of the mechanical displacement remains relatively negligible (first-harmonic assumption [4, 5]).
- The power limit is equal to the sum of all the power limits associated with each mode. This means that the simultaneous exploitation of the multiple modes of the energy harvester allows to harvest more power than the traditional power limit that is associated with a single mode [5]. This phenomenon where the harvested power can go beyond the single-mode power limit is referred as multi-modes resonance.

C. Optimal voltages across the electodes

Because they are both periodic functions, the mechanical displacement associated with the n^{th} mode and the piezoelectric voltage across the m^{th} electrode can be expressed as the sums of in-phase and out-of-phase components: $x_n = \sum_{k=1}^{+\infty}[a_k^n \cos(k\omega t) + b_k^n \sin(k\omega t)]$ and $v_m = \sum_{k=1}^{+\infty}[c_k^m \cos(k\omega t) + d_k^m \sin(k\omega t)]$. Combining these expressions with (1) and replacing a_k^n and b_k^n by their optimal values given by (8) lead to optimality conditions on the electrodes voltages components, c_k^m and d_k^m.

$$\begin{cases} \forall n, \quad \displaystyle\sum_{m=1}^{M}\alpha_{nm} c_1^m = \frac{\gamma_m B_{f_n} Q_n(\Omega_n^2 - 1)}{2\Omega_n} \\ \forall n, \quad \displaystyle\sum_{m=1}^{M}\alpha_{nm} d_1^m = -\frac{B_{f_n}\gamma_m}{2} \\ \forall k > 1, \forall n, \quad \displaystyle\sum_{m=1}^{M}\alpha_{nm} c_k^m = \sum_{m=1}^{M}\alpha_{nm} d_k^m = 0 \end{cases} \tag{10}$$

From (10), one can draw the following conclusions:

- In order to attain the power limit P_{lim} with N resonance modes, $2N$ conditions should be met by the piezoelectric voltages across all electrodes. In order to respect all these conditions, the number of electrodes should be equal or greater than the number of modes considered ($M > N$).

- The third equation of (10) shows that the harmonics linked with a single electrode can be compensated by the harmonics linked with another electrode, in order to reach the power limit even if the electrical interface is non-linear. This mean that some electrodes can be used to suppress the harmonic influences of other electrodes, avoiding harmonic generation on the mechanical displacement.

III. Analysis of the Harvested Power on a Resistor

It is not always possible to respect the optimality conditions given by (8) and (10) when the vibration frequency is far from one of the mode resonance frequency. To investigate this, a harvester of two modes ($N = 2$) and two electrodes ($M = 2$) is considered. The mechanical and electrical dynamics of such system are given by (11) and (12),

$$\begin{cases} M_1 \dfrac{d^2x_1}{dt^2} + D_1 \dfrac{dx_1}{dt} + K_1 x_1 + \alpha_{11} v_1 + \alpha_{12} v_2 = B_{f_1} \gamma \\ M_2 \dfrac{d^2x_2}{dt^2} + D_2 \dfrac{dx_2}{dt} + K_2 x_2 + \alpha_{21} v_1 + \alpha_{22} v_2 = B_{f_2} \gamma \end{cases} \tag{11}$$

$$\begin{cases} i_1 = \dfrac{v_1}{R_1} = C_{p_1} \dot{v}_1 - \alpha_{11}\, \dot{x}_1 - \alpha_{21}\, \dot{x}_2 \\ i_2 = \dfrac{v_2}{R_2} = C_{p_2} \dot{v}_2 - \alpha_{12}\, \dot{x}_1 - \alpha_{22}\, \dot{x}_2 \end{cases} \tag{12}$$

where R_1 and R_2 correspond to the resistive loads connected to the electrodes 1 and 2, respectively. Note that in the particular case where the two electrodes are in parallel, the two currents i_1 and i_2 can be summed and the total current is: $v/R = \left(C_{p_1} + C_{p_2}\right) \dot{v} - \alpha_{11}\, \dot{x}_1 - \alpha_{21}\, \dot{x}_2 - \alpha_{12}\, \dot{x}_1 - \alpha_{22}\, \dot{x}_2$

From (12), the relation in frequency domain between the voltage across each electrode and the displacement of each mode can be obtained,

$$\underline{v_m} = \frac{\left(\alpha_{1m}\underline{x_1} + \alpha_{2m}\underline{x_2}\right)}{C_{p_m}} \left(\varepsilon_{K_m} + j\varepsilon_{D_m}\right) \tag{13}$$

with ε_{D_m} and ε_{K_m} being the dimensionless electrical-induced damping and stiffness associated with the m^{th} electrode, respectively [13]. Note that the expressions of ε_{D_m} and ε_{K_m} remain identical to the single-mode single-electrode case [13].

$$\begin{cases} \varepsilon_{D_m} = \dfrac{\left(R_m C_{p_m} \omega\right)}{1 + \left(R_m C_{p_m} \omega\right)^2} \\ \varepsilon_{K_m} = \dfrac{\left(R_m C_{p_m} \omega\right)^2}{1 + \left(R_m C_{p_m} \omega\right)^2} \end{cases} \tag{14}$$

From (11) and (13), the expressions of the modal displacements in frequency domain can be found by solving the following system:

$$\begin{cases} B_{f_1}\underline{\gamma} = [A_1 + jB_1]\underline{x_1} + [C + jD]\underline{x_2} \\ B_{f_2}\underline{\gamma} = [A_2 + jB_2]\underline{x_2} + [C + jD]\underline{x_1} \end{cases} \tag{15}$$

with A_k, B_k, C and D ($k \in \{1,2\}$) being given by (16).

$$\begin{cases} A_k = K_k - \omega^2 M_k + \dfrac{\alpha_{k1}^2}{C_{p_1}} \varepsilon_{K_1} + \dfrac{\alpha_{k2}^2}{C_{p_2}} \varepsilon_{K_2} \\ B_k = \omega D_k + \dfrac{\alpha_{k1}^2}{C_{p_1}} \varepsilon_{D_1} + \dfrac{\alpha_{k2}^2}{C_{p_2}} \varepsilon_{D_2} \\ C = \dfrac{\alpha_{11}\alpha_{21}}{C_{p_1}} \varepsilon_{K_1} + \dfrac{\alpha_{12}\alpha_{22}}{C_{p_2}} \varepsilon_{K_2} \\ D = \dfrac{\alpha_{11}\alpha_{21}}{C_{p_1}} \varepsilon_{D_1} + \dfrac{\alpha_{12}\alpha_{22}}{C_{p_2}} \varepsilon_{D_2} \end{cases} \tag{16}$$

The expression of the apparent power of the m^{th} electrode can be expressed from (13):

$$S_m = \frac{v_m v_m^*}{2R_m} \tag{17}$$

The harvested power with each electrode P_m is equal to the real part of S_m. Its analytical expression is too long to be given here, but can be easily obtained from (15) and (17). In all the following simulations, the values of the dimensional parameters ($M_1, M_2, D_1, D_2, \ldots$) are chosen to obtain $Q_1 = Q_2 = 50$, $\omega_2 = 2\omega_1 = 200\, rad.s^{-1}$, and $P_{\lim}^1 = 2P_{lim}^2$. The values of the four normalized coupling $k_m^2|_{nm} = \alpha_{nm}^2/(K_n C_{p_m})$ corresponding to the electromechanical coupling between the n^{th} resonance mode with the m^{th} piezoelectric electrode, are given for each simulation.

Figure 3 shows the maximum total harvested power (with the two electrodes) with optimized resistances R_1 and R_2 as a function of the vibration frequency, with $k_m^2|_{11} = k_m^2|_{22} = 0.2$, and $k_m^2|_{12} = 0$. The blue curve shows the maximum power when the coupling between the first electrode and the second mode is null ($k_m^2|_{21} = 0$). In this case, the power does not go beyond the power limit $P_{\lim}^1$. In the other hand, when a non-null coupling is introduced in the simulation ($k_m^2|_{21} = 0.1$), the maximum power goes beyond P_{lim}^1 from about 18%. Such simple example illustrates how a bi-modal resonance can appear thanks to multi-modes coupling. The increase of power around this bi-modal resonance is due to the charges generated from the mechanical displacement of the second mode that is in-phase with the mechanical displacement of the first mode. Even though the second mode displacement remains small (because the bi-modal resonance frequency is far from the second mode resonance frequency), the small voltage generated by this displacement adds up with the already-large voltage generated by the displacement of the first mode. Therefore, the harvested power is greatly increased, because it is quadratically related to the total voltage. Note that the closest the two modes frequencies are, the greater the power around the bi-modal resonance.

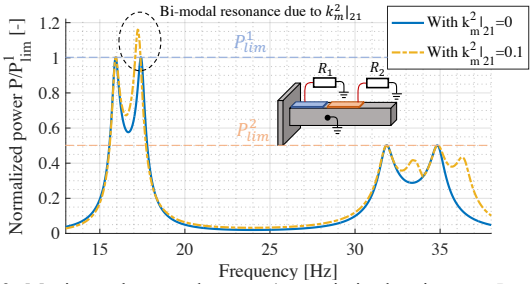

Figure 3: Maximum harvested power (on optimized resistances R_1 and R_2) with $k_m^2|_{11} = k_m^2|_{22} = 0.2$ and $k_m^2|_{12} = 0$. The blue curve shows the maximum power with no coupling between the second mode and first electrode ($k_m^2|_{21} = 0$) while the yellow curve shows the maximum power with $k_m^2|_{21} = 0.1$.

Figure 4 shows that such bi-modal resonance can be obtained even if $k_m^2|_{21} = k_m^2|_{12} = 0$, as long as the two electrodes are connected in parallel. Indeed, when the electrodes are connected in parallel, the electromechanical coupling $k_m^2|_{22}$ leads to a non-null coupling between the two electrodes with the second mode, which enables the existence of a bi-modal resonance. Interestingly, the maximum achievable harvested power with the two parallel-connected electrodes can be greater than the maximum achievable harvested power with the two electrodes when they are not connected in parallel (blue curve in Fig.3).

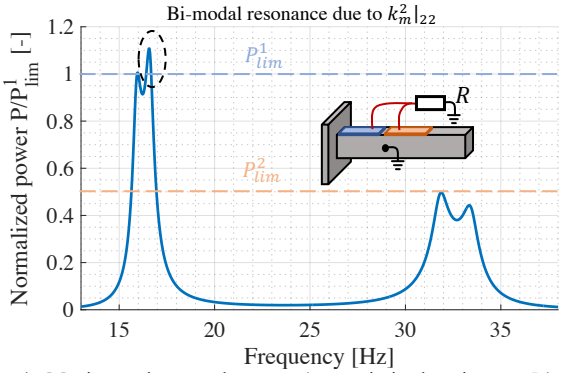

Figure 4: Maximum harvested power (on optimized resistance R) with $k_m^2|_{11} = k_m^2|_{22} = 0.2$ and $k_m^2|_{12} = k_m^2|_{21} = 0$, when the piezoelectric electrodes are connected in parallel.

IV. Experimentations on a Multi-modes Multi-electrodes Harvester

A. Custom-made energy harvester

In order to validate the proposed concepts, a multi-modes multi-electrodes piezoelectric energy harvester has been designed. As shown in Fig.5, the harvester is made with a cantilever beam of steel covered by four pairs of electrodes of soft piezoelectric ceramics PZT (its fabrication being detailed in [14]). As shown in Fig.5, the inertial mass of the harvester is inverted in order to bring closer the resonance frequencies of the first and second modes.

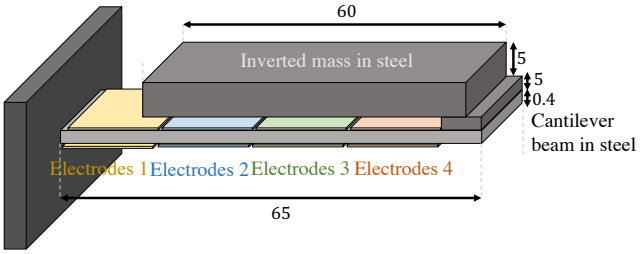

Figure 5: Experimental realization of a multi-modes multi-electrodes energy harvester. Dimensions are indicated in millimeters.

B. Experimental set-up

The designed prototype has been fixed on an electromagnetic shaker. As shown in Fig.6, the acceleration of the electromagnetic shaker is sensed thanks to an accelerometer, whose output is sent to a dSpace control board. The input of the power amplifier (that drives the electromagnetic shaker) is also sent from the same dSpace board and the amplitude of this signal is adjusted internally in dSpace thanks to a PI controller, in order to always maintain the acceleration amplitude to 0.1m.s^{-2}. The displacement and speed of the tip of the harvester are sensed thanks to a vibrometer laser, and the voltage across the electrodes is sensed thanks to a unity-gain amplifier whose output is sent to dSpace. The electrodes are also connected to a programmable resistance decade box whose value is directly sent from the dSpace board.

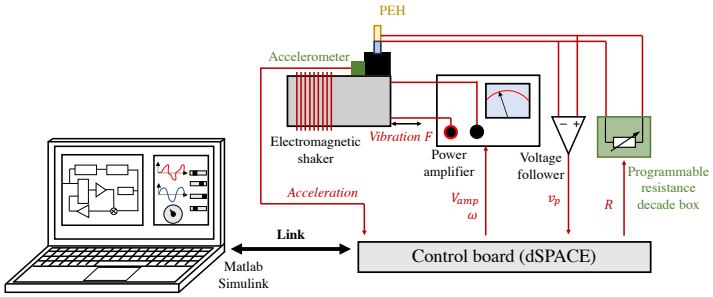

Figure 6: Experimental setup for the test of the multi-modes multi-electrodes energy harvester.

C. Experimental characterization of the prototype

In order to characterize each mode from each piezoelectric port, each pair of piezoelectric electrodes has been successively connected to 20 resistive loads while all the other electrodes were short-circuited, and the PEH has been excited with 60 vibration frequencies. The measured displacement as well as the measured power have been used to find the characteristics of each mode seen from each piezoelectric port thanks to a fitting algorithm on Matlab. From these characterizations, the following parameters of the multi-modes multi-electrodes PEH have been identified:

TABLE I. Identified parameters of the multi-modes multi-electrodes piezoelectric energy harvester

Parameters	Values				Units
	$m = 1$	$m = 2$	$m = 3$	$m = 4$	
α_{1m}	2.3	1.3	0.54	0.070	mN.m^{-1}
α_{2m}	-2.9	-2.4	-7	-12	mN.m^{-1}
C_{p_m}	39	41	34	31	nF
$k_m^2\|_{1m}$	0.087	0.026	0.0055	1.0×10^{-4}	-
$k_m^2\|_{2m}$	0.0034	0.0022	0.023	0.073	-
M_1	33				g
M_2	580				g
B_{f_1}	178				g
B_{f_2}	735				g
Q_1	45				-
Q_2	40				-
ω_1	217.4				rad.s^{-1}
ω_2	332				rad.s^{-1}
P^1_{lim}	245				µW
P^2_{lim}	144				µW

$k_m^2|_{nm} = \alpha_{nm}^2/(K_n C_{p_m})$ corresponds to the expedient electromechanical coupling between the n^{th} resonance mode and the m^{th} pair of piezoelectric electrodes. Because of the low-coupling of some combinations of electrode/mode (e.g., second electrode with second mode), the low identified values of α and k_m^2 might be approximative. We can observe that the first pair of electrodes exhibits the largest coupling with the

first mode, while the fourth pair of electrodes exhibits the largest coupling with the second mode, which is coherent with the literature on the subject [2]. Because of the inverted mass of the harvester, the resonance frequencies of the first and second modes are relatively close ($\omega_1 = 217.4\, rad.s^{-1}$, $\omega_2 = 332\, rad.s^{-1}$), and the power limits of both modes are of the same order of magnitude.

D. Experimental results

Figure 7 shows the maximum power with each mode (with the optimal resistive load maximizing the harvested power) as a function of the vibration frequency. As shown in Fig.7, the power limit of the first mode P_{lim}^1 is only obtained with the first pair of electrodes, because its coupling is large enough and respects the condition $k_m^2|_{11} > 2/Q_1$ [13]. Similarly, the only pair of electrodes that allows to reach the power limit of the second mode (P_{lim}^2) is the fourth one, because $k_m^2|_{24} > 2/Q_2$ [13].

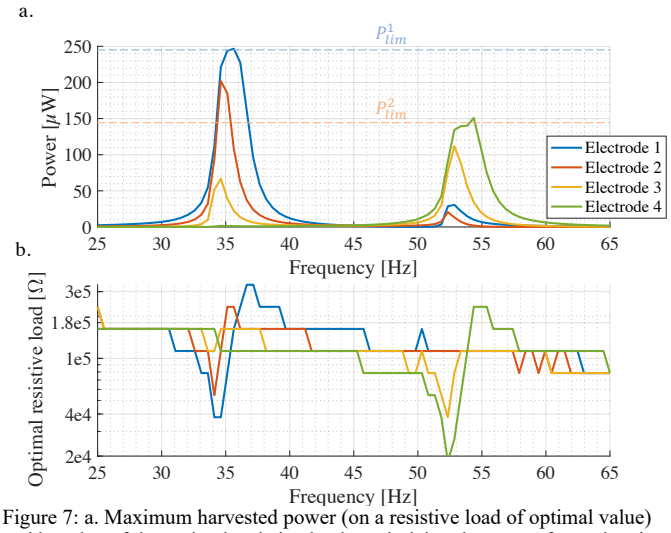

Figure 7: a. Maximum harvested power (on a resistive load of optimal value) and b. value of the optimal resistive load maximizing the power for each pair of electrodes, with $\gamma_m = 0.1m.s^{-2}$.

Figure 7 shows that the proposed multi-modes multi-electrodes harvester allows to harvest a relatively large power, up to 250 μW (resp. 150μW) for the first (resp. second) mode resonance. Another advantage of the proposed harvester can be seen from Fig.7.b: for a given vibration frequency, the optimal resistive load maximizing the harvested power depends on which pair of electrodes is connected to the electrical circuit. Therefore, it is also possible to optimize the harvested power by adjusting the configurations of the connected electrodes to the electrical circuit, as demonstrated in [15].

When the four pair of electrodes are connected in parallel, the equivalent electromechanical coupling with the first mode $k_m^2|_1$ and second mode $k_m^2|_2$ can be predicted using (16).

$$k_m^2|_n = \frac{\left(\sum_{m=1}^{M} \sqrt{k_m^2|_{nm} C_{p_m}}\right)^2}{\sum_{m=1}^{M} C_{p_m}} \tag{16}$$

The coupling of the first mode $k_m^2|_1$ is equal to 0.078, while the coupling of the second mode $k_m^2|_2$ is equal to 0.064. This means that both modes respect the condition $k_m^2|_i Q_i > 2$ and that the harvested power with an optimal resistive load should reach both P_{lim}^1 and P_{lim}^2 [13]. Figure 8 shows the harvested power in this configuration (four pairs of electrodes connected in parallel) as a function of the vibration frequency. Figure 8 confirms that both power limit P_{lim}^1 (around ω_1) and P_{lim}^2 (around ω_2) can (almost) be reached. Figure 9 shows the maximum harvested power (on an optimal resistance) around the first mode resonance frequency, with more resistance values (20 in Fig.8, 60 in Fig.9) and a smaller frequency step (0.5 Hz in Fig.8, 0.2 Hz in Fig.9)

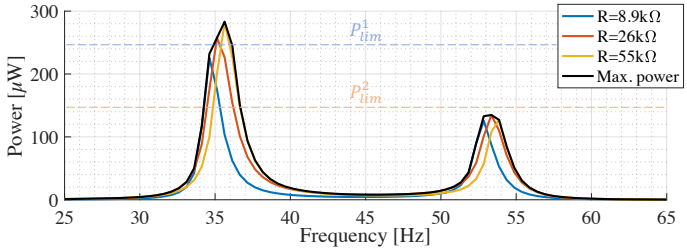

Figure 8: Harvested power with the four pairs of electrodes connected in parallel as a function of the vibration frequency.

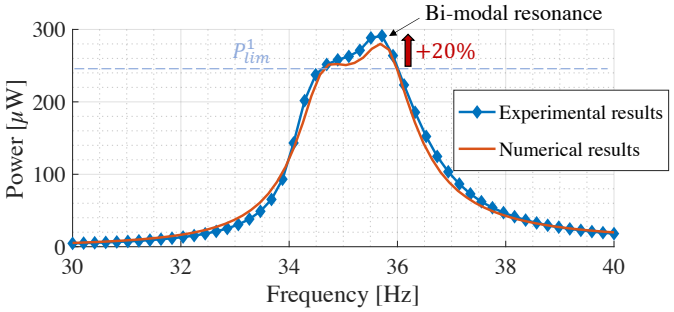

Figure 9: Maximum harvested power (on a resistive load of optimal value) with the four pairs of electrodes in parallel, around the first resonance mode, illustrating the bi-modal resonance phenomenon.

Figure 9 reveals a particularly interesting phenomenon that was predicted by equation (9). Around 35.5 Hz, the harvested power goes beyond the traditional power limit P_{lim}^1 and grows to 294μW (20% more than P_{lim}^1). This power peak is due to the existence of a bi-modal resonance, and is well-predicted by the model proposed in section III of this paper (14)-(15) (Fig.3 and Fig.4). This phenomenon shows that the influence of higher resonance modes can be positive, even though these influences are often seen as negative in the piezoelectric-based conversion [16] and piezoelectric energy harvesting literatures [4][5]. Such phenomenon allows to expand the power limit of multi-modes structures with little-to-no increase of the harvester's volume, which may lead to the design of harvesters exhibiting higher power densities.

V. Conclusion

In this paper, we propose a model for multi-modes multi-electrodes piezoelectric energy harvesters. Based on this model, we prove that the harvested power can be greater than the traditional power limit thanks to multi-modes resonance. Our model as well as the multi-modes resonance phenomenon are validated experimentally, thanks to a 4-electrodes 2-modes piezoelectric energy harvester based on an inverted mass. Such model opens new ways to design strong power-density and large bandwidth piezoelectric energy harvesters thanks to multi-modes resonances and to clever electrode placement/choice.

ACKNOWLEDGMENT

A.M. thanks M.-Y. Durand for the fruitful discussions on dynamics and resonances.

REFERENCES

[1] A. Toprak, O. Tigli, "Piezoelectric energy harvesting: State-of-the-art and challenges", *Applied Physics Reviews*, 1(3), 031104, 2014.

[2] D. Gibus et al., "Strongly coupled piezoelectric cantilevers for broadband vibration energy harvesting", *Applied Energy,* vol. 277, 115518, 2020.

[3] M. Lallart, W.J. Wu, Y. Hsieh, L. Yan, "Synchronous inversion and charge extraction (SICE): a hybrid switching interface for efficient vibrational energy harvesting", *Smart Materials and Structures*, vol. 26, 11, 115012, 2017.

[4] A. Morel, A. Badel, Y. Wanderoild, G. Pillonnet, "A unified N-SECE strategy for highly coupled piezoelectric energy scavengers", *Smart Materials and Structures*, vol. 27, 8, 084002, 2018.

[5] A. Brenes et al., "Maximum power point of piezoelectric energy harvesters: a review of optimality condition for electrical tuning", *Smart Materials and Structures*, vol. 29, 3, 033001, 2020.

[6] E. Halvorsen, C. P. Le, P. D. Mitcheson, and E. M. Yeatman, "Architecture-independent power bound for vibration energy harvesters", in *PowerMEMS*, London, UK, 2013.

[7] Y. Liao, and H. Sodano "Optimal power, power limit and damping of vibration based piezoelectric power harvesters", *Smart Materials and Structures*, vol. 27, 7, 075057, 2018.

[8] A. Erturk, J. M. Renno, D. J. Inman, "Modeling of Piezoelectric Energy Harvesting from an L-shaped Beam-mass Structure with an Application to UAVs", *Journal of Intelligent Material Systems and Structures,* vol. 20, 5, pp. 529-544, 2009.

[9] M. Ferrari, V. Ferrari, M. Guizzetti, et al., "Piezoelectric multifrequency energy converter for power harvesting in autonomous microsystems", *Sensors and Actuators A: Physical*, vol. 142, pp. 329-335, 2008.

[10] L. Tang, Y. Yang, "A multiple-degree-of-freedom piezoelectric energy harvesting model", *Journal of Intelligent Material Systems and Structures,* vol. 23, 14, pp. 1631-1647, 2012.

[11] A. Erturk, D. J. Inman, "Issues in mathematical modeling of piezoelectric energy harvesters", *Smart Materials and Structures*, vol. 17, 6, 065016, 2008.

[12] Y. Jia, "Review of nonlinear vibration energy harvesting: Duffing, bistability, parametric, stochastic and others", *Journal of Intelligent Material Systems and Structures,* vol. 31, 7, pp. 921-944, 2020.

[13] A. Morel et al., "Resistive and reactive loads' influences on highly coupled piezoelectric generators for wideband vibrations energy harvesting", *Journal of Intelligent Material Systems and Structures*, vol. 30, 3, pp. 386-399, 2019.

[14] D. Gibus et al., "Design of a vibration energy harvester with two close resonant frequencies", *IEEE Wireless Power Week (WPW) 2022*, *in press*, 2022.

[15] S. Du, Y. Jia, A. A. Seshia, "Piezoelectric vibration energy harvesting: A connection configuration schema to increase operational range and output power", *Journal of Intelligent Material Systems and Structures,* vol. 28, 14, pp. 1905-1915, 2016.

[16] L. D. A. Pereira et al., "Operating frequency prediction of piezoelectric dc-dc converters", IEEE Transactions on Power Electronics, vol. 37, 3, pp. 2508-2512, 2022.